Transfers Between L1 and L2 in the Earth-Moon System

Rohan Patel *

December 2022

Abstract

Transfers between the Earth-Moon L1 and L2 Lagrange points are presented in this work along with the supporting dynamics. These transfers take into consideration the gravitational perturbations of the Earth and Moon, in assumed circular orbits, through the use of the Circular Restricted Three Body Problem (CR3BP). Specific mission requirements are included which in turn drove the trajectory search and final transfers. Insights from periodic orbit families and their departure and arrival manifolds are applied to find good initial guesses for a multiple shooting method. This algorithm minimizes constraint errors, but does not guarantee an optimal transfer. This paper demonstrates transfer trajectories between two sets of periodic orbits, for a total of four. The first set are between two Lyapunov orbits and the other two are between the L1 Northern Halo and the L2 Southern Halo periodic orbits.

1 Introduction and Motivation

There has been a growing demand for Lunar mission designs from continued interest by international science communities. Technological development and ride-sharing has made missions considerably cost effective. Designers can enable low maneuver cost missions, measured in ΔV, that rely on multi-body dynamics to realize these advancements. In the mission design process, it is ideal to first begin a search space exploration in a lower fidelity dynamical model, then to use the results as a starting point for high fidelity trajectory design. The conventionally used two-body problem can also be used to place spacecraft into conic orbits around the Moon from Earth. While this method is useful, it does not take into account the significant gravitational perturbations caused by the Earth and Moon along the trajectory. Therefore, the Circular Restricted Three Body Problem (CR3BP) can be employed as our starting point. The CR3BP models the forces of a primary and secondary celestial body on the spacecraft, and studying this dynamical environment yields insight into potentially low cost transfers. This model will be used to find potential transfer trajectories to and from varying periodic orbits in the Earth-Moon system.

For this paper, the first mission design is to remain within the plane created by the Earth and Moon orbits. This is a small-sat. following along as a rideshare to an L1 Lyapunov with a Jacobi constant of roughly 3.169. Individual transfers are limited to a ΔV of less than 20 m/s. On the side closest to Earth, continuous communication to Earth and Lunar science is possible. The transfer to the far side of the Moon and the periodic orbit needs to allow for a full mapping of every longitude of the Lunar surface. The initial and final orbits must have a period of less than 15 days about their respective Lagrange points for operations purposes, however the transfer time is unconstrained. A second mission design is to have inclined science orbits to study higher Lunar latitudes. There is no time constraint on the science orbits or the transfer. This mission is constrained by a lunar conjunction duration of up to 5 hours due to a requirement for communication and operations to and from the Earth.

In this paper, we will address these requirements with orbit selection and transfer design. First, the system dynamical model and periodic orbits generation is discussed. Then a strategy to find potential periodic orbits and transfers is shown. Finally, the transfers are presented with analysis and future work.

*Masters Student, Aerospace Engineering Department, ASEN6060 Fall 2022

2 System Dynamical Model

2.1 Governing Equations of Motion

The transfer design is investigated in the Circular Restricted Three Body Problem (CR3BP). In this paper, the derivations of the CR3BP and its components is not presented. However, the resulting equations of motion and other useful properties are shown in this section. The CR3BP exhibits certain symmetries that we can utilize which is discussed further on. This dynamical model incorporates the gravitational effects of two celestial bodies which will be called the primary and secondary. The paths these bodies take in the system is assumed to be circular about the system's barycenter. We can utilize this simplification to construct a rotating frame that has its x/y plane rotate at the same rate as the rate of the bodies about the barycenter. Therefore, the position of the bodies will always be some x-coordinate and zero for the y and z-coordinates. Because the primary and secondary do not change distances from each other, we can use the radius between the two to non-dimensionalize (ND) the system. Further, the system's period can be used to non-dimensionalize the time quantity. The ND transformations are shown below:

$$l^* = \tilde{R}_1 + \tilde{R}_2 \qquad t^* = \left(\frac{(l^*)^3}{\tilde{G}m^*}\right)^{1/2} \tag{1}$$

where l^* and t^* are the ND length and time conversion factors, $\tilde{R}$ is the dimensional radius of the celestial body from the system barycenter, m^* is the dimensional total mass of the system, and $\tilde{G}$ is the dimensional gravitational constant. Eq.(2) represents the equations of motion governing the path of the spacecraft in the CR3BP:

$$\vec{x}_{rot.} = \begin{bmatrix} x \\ y \\ z \\ \dot{x} \\ \dot{y} \\ \dot{z} \end{bmatrix}_{6\times1} \qquad \dot{\vec{x}}_{rot.} = \begin{bmatrix} \dot{x} \\ \dot{y} \\ \dot{z} \\ 2\dot{y} + \frac{\partial U^*}{\partial x} \\ -2\dot{x} + \frac{\partial U^*}{\partial y} \\ \frac{\partial U^*}{\partial z} \end{bmatrix}_{6\times1} \tag{2}$$

where U is the pseudo-potential function shown in Eq.(3); r_1 and r_2 are the magnitudes of the vectors from the primary and secondary to the spacecraft respectively. Recall that all state and time quantities are non-dimensional.

$$U^* = \frac{1}{2}(x^2 + y^2) + \frac{1-\mu}{r_1} + \frac{\mu}{r_2} \tag{3}$$

We can utilize the state transition matrix (STM) to linearly map perturbed initial states. Doing so will be useful during our update scheme to correct the initial guess trajectories. The STM consists of the partials of each final state element with respect to the initial ones either forwards or backwards in time (Δt). Therefore, the initial conditions for the STM is simply an identity matrix, and it is propagated using the Jacobian of the dynamical system ($[A]$). With this in mind, we can rewrite the equations of motion, with the STM (Φ) as follows:

$$\vec{x} = \begin{bmatrix} x \\ y \\ z \\ \dot{x} \\ \dot{y} \\ \dot{z} \\ \Phi(\Delta t, 0) \end{bmatrix}_{42\times1} \qquad \dot{\vec{x}}_{rot.} = \begin{bmatrix} \dot{x} \\ \dot{y} \\ \dot{z} \\ 2\dot{y} + \frac{\partial U^*}{\partial x} \\ -2\dot{x} + \frac{\partial U^*}{\partial y} \\ \frac{\partial U^*}{\partial z} \\ [A]\Phi(\Delta t, 0) \end{bmatrix}_{42\times1} \tag{4}$$

Note that the STM is a 6×6 matrix, but in the equations of motion it is reshaped to a 36×1 vector for proper matrix dimensions. An STM that maps one revolution of a periodic orbit is called the monodromy matrix. This will be handy when designing the departure and arrival to and from POs.

Within the CR3BP, five equilibrium points, also referred to as Lagrange points, exist. These states have a zero velocity and acceleration components. The mathematical formulation of these points is not covered in this paper, however, their locations are provided graphically in Figure 1. Each Lagrange

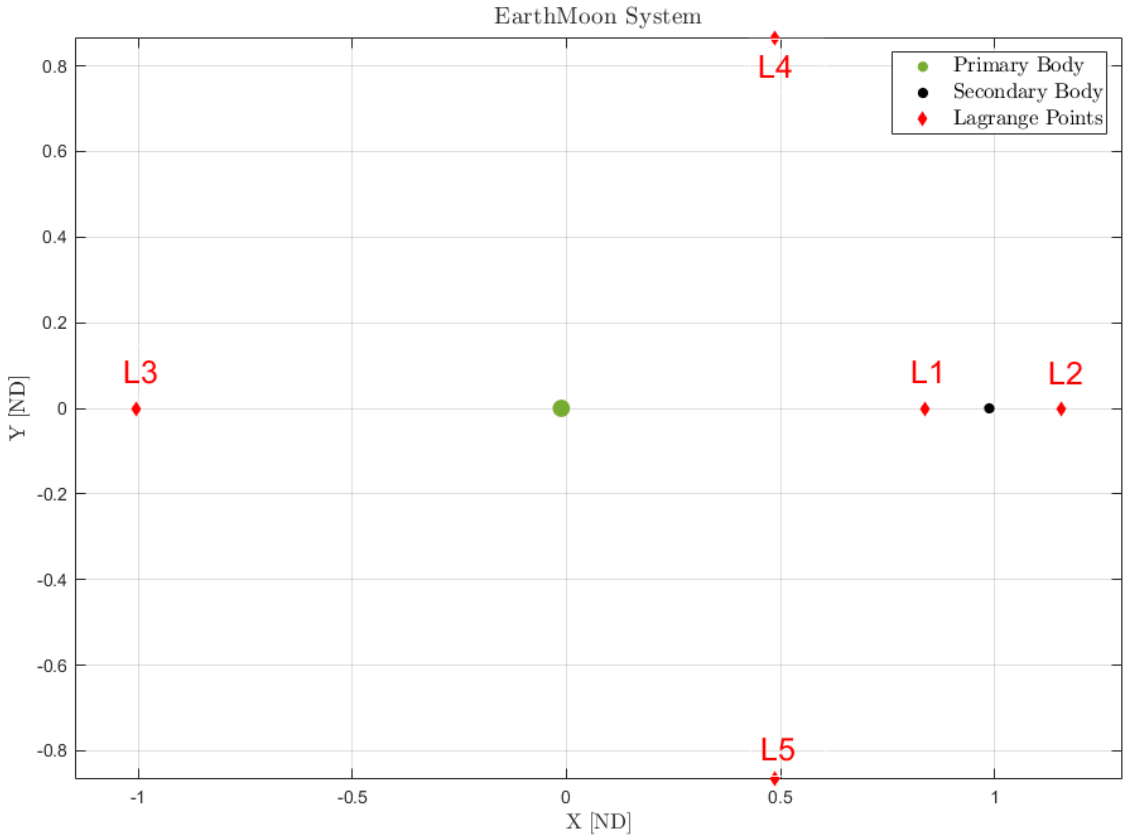

Figure 1: Locations of all five Earth-Moon system equilibrium points.

point is denoted by an "L" followed by the corresponding number. L1 and L2 are relatively close to the secondary body, the Moon. L3 is furthest away from the Moon. L4 and L5 form equilateral triangles with the Earth, Moon, and Lagrange points making up each side. For this paper, we are interested in periodic orbits (PO) around L1 and L2.

2.2 Periodic Orbits Around L1 and L2

Different families of periodic solutions exist about various locations in the CR3BP. In this study, we will focus on two types of periodic orbit (PO) families around both the L1 and L2 Lagrange points. Generating these families of orbits requires correction of a rough initial guess. This scheme is not presented in this paper, but the results of it and continuity are presented in this section. Correction is an iterative process that adjusts the initial guess state and integration time such that the final state returns to the initial to within a specified tolerance. Correction is done from the mirror-theorem which leverages the symmetries of orbits about the x-axis in the CR3BP. A more robust method of correction is the general-variable time theorem which can be employed as either a single or multiple shooting scheme. Continuity allows us to step from one completed PO to a family of them by either: 1) natural parameter continuation, or 2) pseudo-arclength continuation. The implementation of these methods won't be discussed in this paper, but at a high level, both methods offer a way to perturb an already converged PO initial guess to find another guess in the close vicinity of the existing PO. Then applying correction, a new PO is generated.

By applying these methods we are able to generate the useful PO families for our mission designs. Figure 2 shows the Lyapunov (top subfigure) and the L1 Northern Halo and L2 Southern Halo orbit family (bottom subfigure). Note that the Lyapunov family plot is zoomed into the vicinity of the Moon as this is likely where our mission satisfying periodic orbits will exist. Both are color coded by each PO's Jacobi constant. The next step is to narrow down the search space to single orbits.

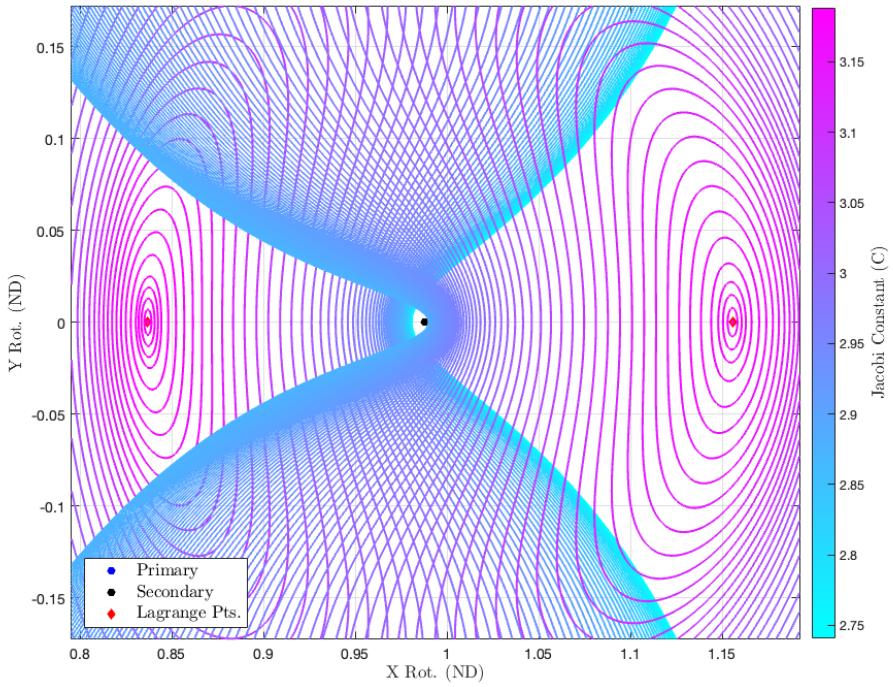

(a) L1 and L2 Lyapunov Periodic Orbit Families (primary body not in axis limits).

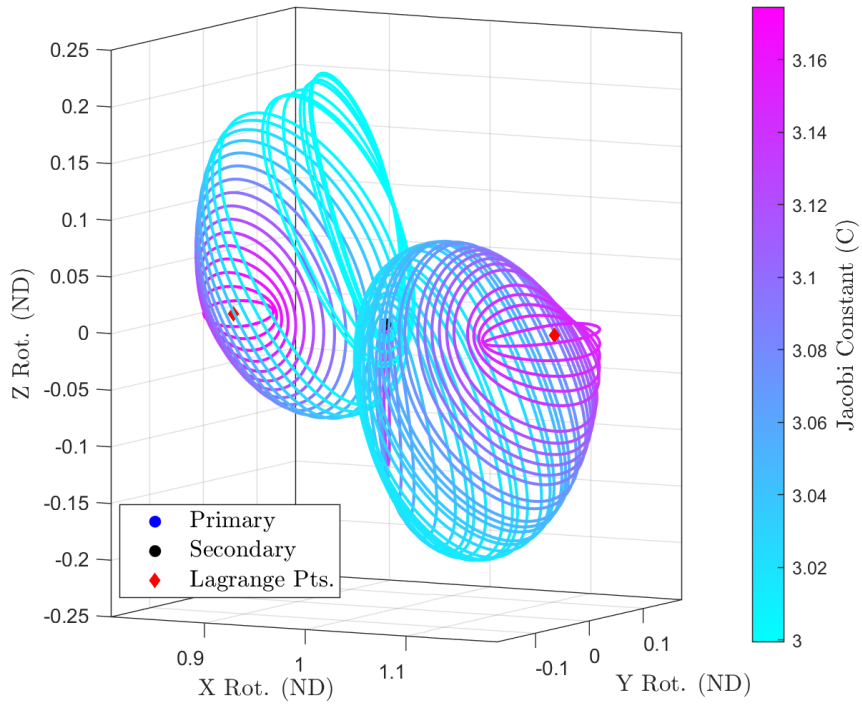

(b) L1 Northern and L2 Southern Halo Periodic Orbit Families (primary body not in axis limits).

Figure 2: Lyapunov and Halo families color coded by Jacobi constant. These PO families will satisfy the study's two mission designs requirements.

3 Problem Formulation

3.1 Periodic Orbit Selection

The periodic orbit solutions discussed in the previous section enable endless opportunities for initial and terminal orbits. Therefore, we can use the requirements and insights from their manifolds to narrow down the selection process. This and the next sub-section, which outlines manifolds and their use for transfer initial guesses, are closely intertwined. An iterative process was used to find potential periodic orbits. The process includes: 1) selecting candidate POs that at least satisfy the non-maneuver cost or conjunction mission requirements, 2) checking the departing and arriving manifolds of said POs, 3) verifying if these manifolds yield a solution that satisfies all the requirements. With this in mind, it is important to note that there is likely other periodic orbit pairs that will satisfy all the requirements of this research, but for the sake of time and brevity, the first set of pairs found to completely satisfy both mission design's requirements are kept and shown below.

Design "A" includes Transfer 1A and 2A; let us address the first mission design with these transfers. From the previous section, Lyapunov orbits are planar with respect to the Earth-Moon orbits. This serves as a great candidate for the science orbits and transfer design. A hard requirement of science orbits being less than 15 days means that we can filter out all Lyapunov solutions shown in Figure 2 that have a period of greater than 3.4542 non-dimensional units. Next, because of the ridesharing constraint, our L1 periodic orbit must have a Jacobi constant relatively close to 3.169. After looking at several potential transfer manifolds, which are outlined in the next section, a set of L1 and L2 Lyapunov periodic orbits are chosen. The L1 Lyapunov will have a Jacobi constant of 3.16916 corresponding to a period of 12.000 days, and the L2 Lyapunov will have a Jacobi constant of 3.17010 with a period of 14.665 days. The L1 and L2 Jacobi constants do not match exactly, but the values are kept reasonably close to prevent the possibility of having large maneuver costs. This should satisfy the requirement of having individual transfers having less than 20 m/s of ΔV.

Design "B" includes Transfer 1B and 2B which will satisfy the second mission design's requirements. Halo periodic orbits are essential here due to their inclination. In testing with their subsequent manifolds, it was found that Halos that were closer to their respective Lagrange point, and with higher Jacobi constants in the full family, had manifolds that more closely intersected. These are discussed in the next subsection. No mission design requirements specify the maximum height above the Earth-Moon X/Y-plane; therefore, convenient periodic orbits were selected. In testing it was found that transfers from the L1 Northern Halo family had closer manifold intersection conditions to the L2 Southern Halo family and vice versa. Due to the less strict nature of this design, the first set of periodic orbits to satisfy the requirements was used. The L1 Northern Halo and L2 Southern Halo will have a Jacobi constants of 3.1736 and 3.1518 and periods of 24.657 and 20.0187 days respectively.

3.2 Manifolds for Transfer Initial Guesses

We can use insights from the CR3BP to form good initial guesses for transfers. Stable and unstable manifolds exists departing and arriving periodic orbit solutions in the CR3BP. These itineraries allow for very low cost departures and arrivals to our initial and final periodic orbits. At least for the periodic orbit families we are interested in, manifolds often intersect with each other. The entire process to compute manifolds is not discussed in detail, but generally manifolds are generated by utilizing stability information which is found by evaluating the eigen-values of the monodromy matrix. Stable or unstable eigen-vectors can then be used to perturb any arbitrary state along a periodic orbit such that the respective manifold is achieved. Note that eigen-vectors can either be recomputed at the state of interest, or be propagated using the STM computed from the initial PO state to the desired state. A scaling term is applied to the perturbation to ensure the manifold initial condition is sufficiently close to its respective state along the PO.

Departing manifolds are propagated in forwards time, and arriving manifolds are propagated in backwards time to show how the manifold approaches the PO. This is important to note because in the initial guess generation process the integration times need to be flipped accordingly to ensure the trajectory flows correctly. It must go from the departing manifold, to the end of the arriving manifold, and finally to the intended periodic orbit. In order for us to use the unstable departure and stable arrival manifolds for our transfer design, we need to ensure that at least a pair of the intermediate states for both manifolds is sufficiently close to each other. It is unlikely to find a purely hetero-clinic

connection, meaning no discontinuities from one manifold to the other. Therefore, we can resolve these through the multiple shooting process and with impulsive midcourse maneuvers. The paths of these manifolds are mapped out in time to see if this condition is generally met.

Poincaré mapping helps to categorize the search space of manifolds and their intersections. These maps essentially plot selected states at a specific hyperplane and reduce the search free states by one variable. For example, for Lyapunov periodic orbits Z and dZ are always zero. Therefore, the search space for the manifolds is four free variables. If we set up a Poincaré map at the Y/Z hyperplane formed at $x = 1 - \mu$, the Moon's x-coordinate, then the total free states is now down to three. Visualizing in three dimensions is considerably easier than in four. For this example, the X/Y axes can represent the Y and dY coordinates, and a color can signify the dX. Marker shapes can indicate whether the state is on the departure or arrival manifold.

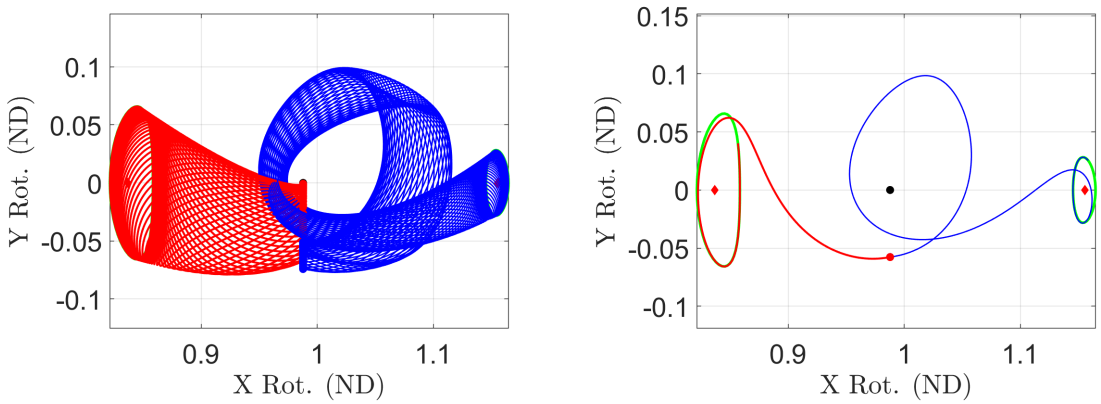

Figure 3: Transfer 1A unstable departure from L1 (red) and stable arrival manifold to L2 (blue).

For Transfer 1A and 2A we need to address the requirement of total longitudinal survey of the Lunar surface. Therefore, our transfers must include a revolution around the Moon in both directions. One or both manifolds can be propagated for long enough such that this condition is achieved. In the integration setup, the manifold states are propagated to the $x = 1 - \mu$ hyperplane and crossings of it are recorded to generate Poincaré maps. Figure 3 visually depicts the unstable departure manifold (red) from the L1 Lyapunov orbit. Integration is terminated at the first encounter of the hyperplane. To satisfy the global longitudinal requirement, the stable arrival manifold (blue) is propagated for multiple passes of the hyperplane to form a single revolution. Notice that the manifolds approach similar Y (ND) values below the Moon at this hyperplane. For Transfer 1A, visual inspection is used to find sufficiently close terminal states of these manifolds to form an initial guess. This guess is shown in the right hand subfigure. The direction of motion from both manifolds is roughly similar (and so dX and dY are close for a good initial guess). For this transfer Poincaré mapping isn't used, but for the return trajectory it is beneficial.

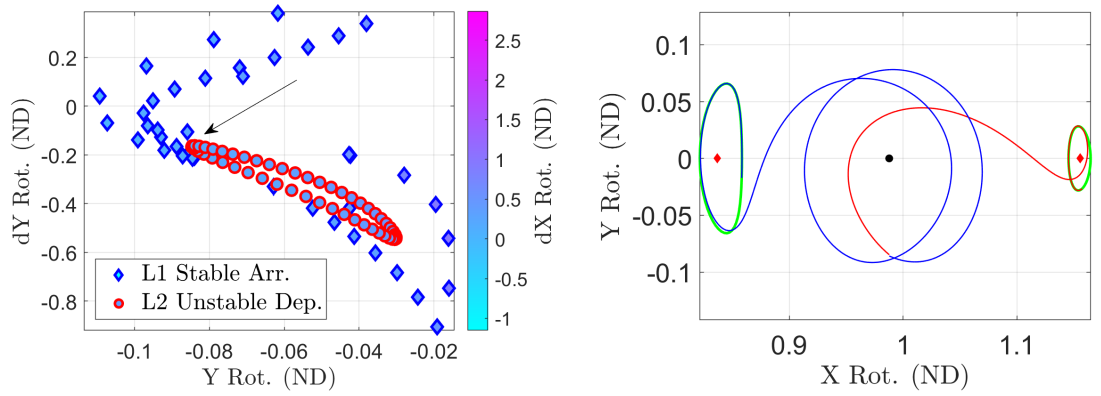

Figure 4: Transfer 2A Poincaré map (left) and selected manifolds for initial guess (right).

Figure 4 shows the transfer design space (left) and the selected initial condition manifolds (right) for the return trajectory for the first mission. To generate this plot, the unstable departure has its first two $x = 1 - \mu$ hyperplane crossings integrated, and the stable arrival has its first four crossings mapped. The figure is zoomed into the region where a potential transfer opportunity exists. The arrow in the subfigure indicates a region of interest, and the manifolds corresponding to these points are shown on the right subfigure. We can confirm that the initial guess manifolds from the Poincaré plot is reasonably close visually and should be able to be corrected through the multiple shooting.

Because Transfers 1B and 2B are between halo periodic orbits, a combination of Poincaré mapping and visual inspection of the manifolds at the $x = 1 - \mu$ hyperplane is required to find suitable initial guesses. Maneuvers can be placed to correct velocity conditions, and so a priority to visualize and closely match position states was given in the initial guess generation process. Poincaré plots created for these transfers had Y and Z (ND) coordinates at the hyperplane plotted on the X/Y axes, and in testing it was seen that variations in dX (ND) component were more useful to visualize. Closer matching dX states led to an easier time finding solutions that the multiple shooting scheme quickly converged on.

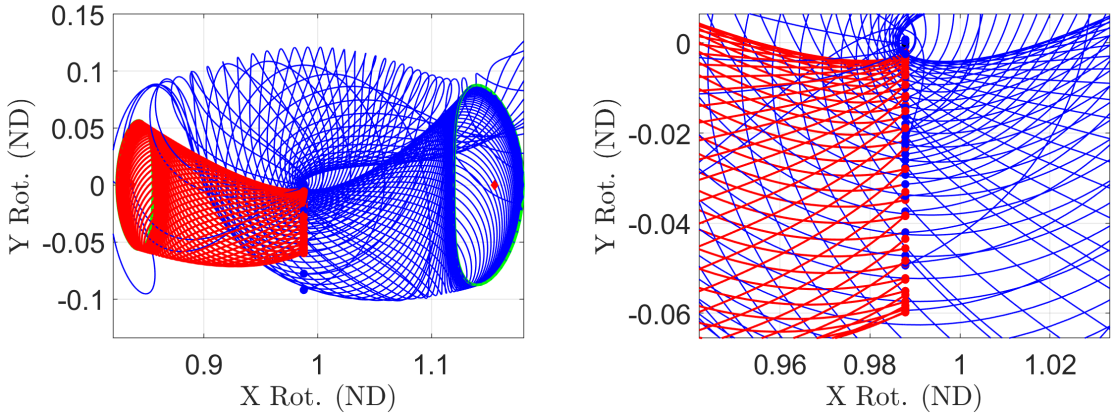

Figure 5: Visualization of manifolds example applied to Transfer 1B.

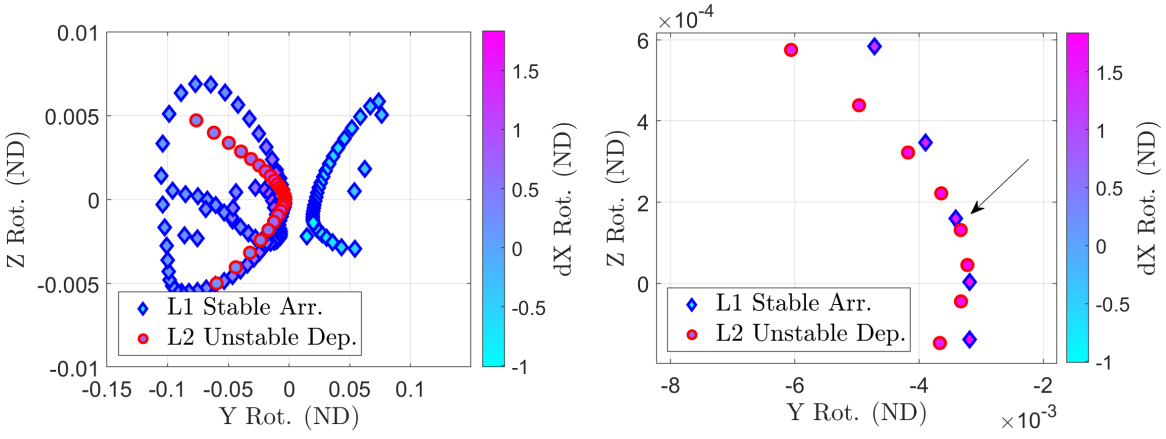

Figure 6: Transfer 2B Poincaré plot. The right subfigure is zoomed in to the manifold pairs of interest.

Figure 5 demonstrates the visualization process applied to Transfer 1B. Figure 6 demonstrates using Poincaré mapping to find Transfer 2B. Note that for both transfers, visualization and mapping was used to find good initial guesses, but for the sake of brevity in this paper, the maps for Transfer 1B and the visualization for Transfer 2B are not shown. Beginning with the visualization process, one or multiple passes of the $x = 1 - \mu$ hyperplane were integrated and plotted in 3-D. Each manifold trajectory was assigned a specific number and crossings of the hyperplane were highlighted with scatter points (as seen in Figure 5 right subfigure). A range of trajectory numbers and their respective number

of passes were recorded to narrow down the search space for the Poincaré mapping process. The maps then offered finer resolution and the ability to compare different state variables (up to five) to find the best initial conditions set. The map in Figure 6 would have been considerably larger if the visualization process wasn't done prior. The right subfigure is the same plot as the left subfigure but zoomed into where the discontinuities in state and x-velocity are smallest (indicated by the black arrow). Figures 12 and 14 show the initial guess manifolds where the red dashed line is the unstable departure and the dark blue dashed line is the stable arrival.

3.3 Initial Guess Correction Using Multiple Shooting

Now that a good initial guess is known for the transfer design, the state discontinuities need to be corrected to produce a continuous trajectory from the periodic orbits. For this study, impulsive maneuvers are considered. Therefore, in selected locations along the trajectory, a discontinuous velocity is acceptable and the difference between velocity states is considered to be the required maneuver. A multiple shooting scheme is useful to correct these discontinuities in a fast and robust manner. Figure

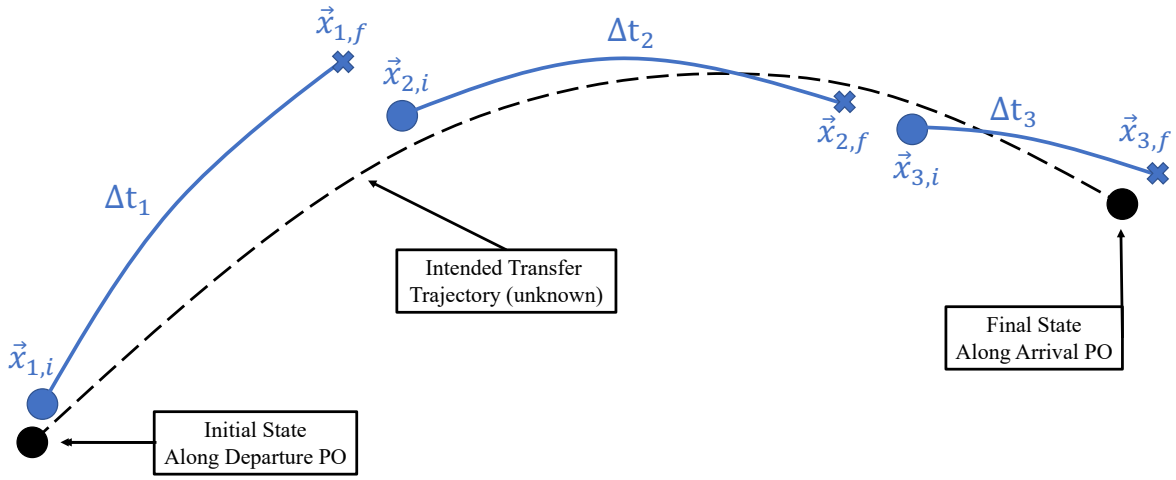

Figure 7: Here is an example diagram of the multiple shooting scheme. Each arc is discontinuous and the initial states for each (denoted by subscript i) need to be corrected such that continuity exists. Note that the true solution, shown as the black dashed line, is reached within some specified tolerance.

7 illustrates the components of a three-segment multiple shooting scheme between initial and terminal conditions along departure and arrival periodic orbits (PO). The scheme attempts to patch intermediate arc discontinuities and thereby reducing the constraints norm to within a specified tolerance. A completed scheme is shown in Figure 8. Here, constraints on position continuity is enforced at every segment, but the velocity is allowed to be discontinuous to model instantaneous maneuvers. The multiple shooting scheme depends on two major components: the free variable vector ($\vec{V}$) and the constraint vector ($\vec{F}(\vec{V})$). The scheme iterates and updates the free variable vector such that the constraints function vector norm is under a specified tolerance value, implying that the constraints imposed on the problem are satisfied. For the transfer problem, we can begin by defining the free variable vector as the non-dimensional states and integration time between segments that comprise of the transfer. The left-hand expression in Eq.(5) shows the free variable vector for a single arc (j) along the trajectory.

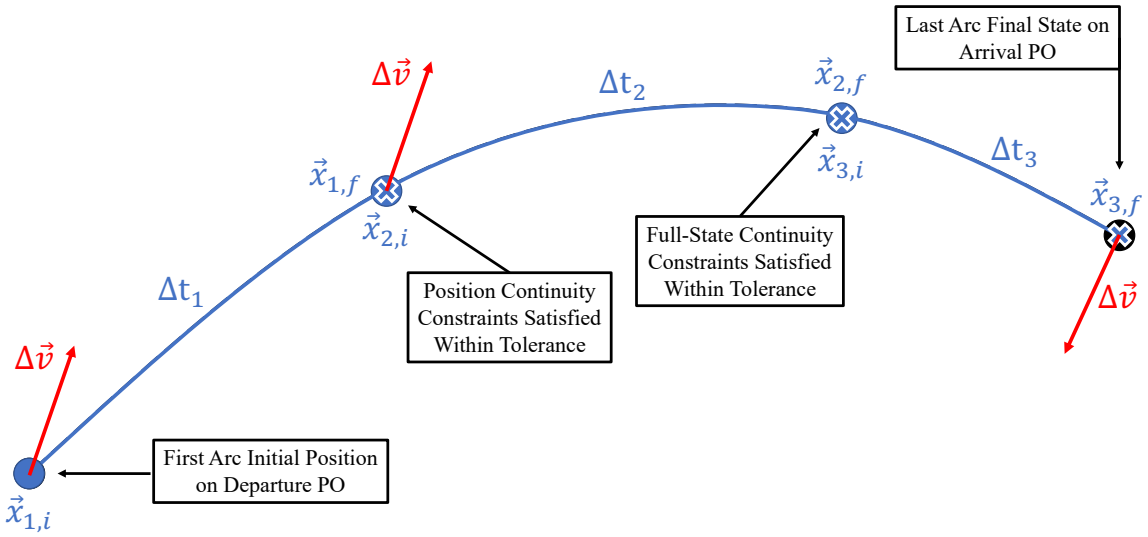

Figure 8: Diagram of recovered solution that has discontinuities within a specified tolerance. In this example, the initial and final states are allowed to have discontinuous velocities which implies maneuvers would be performed to depart and arrive on the POs.

$$\vec{V}_j = \begin{bmatrix} x_j \\ y_j \\ z_j \\ \dot{x}_j \\ \dot{y}_j \\ \dot{z}_j \\ \Delta t_j \end{bmatrix}_{7\times 1} \qquad \vec{V} = \begin{bmatrix} \vec{V}_1 \\ \vec{V}_2 \\ \vdots \\ \vec{V}_n \end{bmatrix}_{7n\times 1} \tag{5}$$

The complete free variable vector ($\vec{V}$), shown on the right, consists of stacking each arc's free variable vector. The total number of arcs along the trajectory is denoted by n. Now that the updating variables vector is defined, we can define a set of constraints to follow the continuity in the trajectory discussed above. These are defined by a constraint function vector that ensures that the final state for the current arc (j) matches the initial state of the next arc ($j+1$). If no maneuver is conducted, then all six state variables must be matched. Similarly, the starting and ending states along the periodic orbit need to be matched as well. The dimensions for the individual constraint vectors are either: 3×1 or 6×1. The individual (left) and total (right) constraint vectors are shown in Eq.(6).

$$\vec{F}(\vec{V})_j = \begin{bmatrix} x_{j,f} - x_{j+1,i} \\ y_{j,f} - y_{j+1,i} \\ z_{j,f} - z_{j+1,i} \\ \dot{x}_{j,f} - \dot{x}_{j+1,i} \\ \dot{y}_{j,f} - \dot{y}_{j+1,i} \\ \dot{z}_{j,f} - \dot{z}_{j+1,i} \end{bmatrix}_{6\times 1} \qquad \vec{F}(\vec{V}) = \begin{bmatrix} \vec{F}(\vec{V})_I \\ \vec{F}(\vec{V})_1 \\ \vdots \\ \vec{F}(\vec{V})_n \end{bmatrix} \tag{6}$$

Note that in Eq.(6) I denotes matching the initial periodic orbit's state. The pre-integrated first arc position and(or) velocity is used against the periodic orbit's state to form the first constraint ($\vec{F}(\vec{V})_I$).

$$\vec{V}_{k+1} = \vec{V}_k - \rho(D\vec{F}(\vec{V}_k)^T[D\vec{F}(\vec{V}_k)D\vec{F}(\vec{V}_k)^T]^{-1}\vec{F}(\vec{V}_k)) \tag{7}$$

The total free variable vector is updated using a minimum-norm solution from Newton's Method. This update is shown in Eq.(7) where the current iteration is (k) and the next is ($k+1$). The update term

can be scaled by the arbitrary constant (ρ). For this method to apply, we must assume that at the current iteration, the solution is sufficiently close to the desired solution. $D\vec{F}(\vec{V}_k)$ is the Jacobian of the constraints with respect to the free variables and is assumed to be invertible. Note that this first-order approximation and so iterations will be required to reach the desired conditions. We expect quadratic convergence because we are using Newton's method for the update. For clarity, the Jacobian matrix is shown in it's sub-matrix blocks below:

$$D\vec{F}(\vec{V}) = \frac{\partial \vec{F}}{\partial \vec{V}} = \begin{bmatrix} \frac{\partial \vec{F}_1}{\partial \vec{V}_1}, \frac{\partial \vec{F}_1}{\partial \vec{V}_2}, \dots, \frac{\partial \vec{F}_1}{\partial \vec{V}_n} \\ \frac{\partial \vec{F}_1}{\partial \vec{V}_1}, \frac{\partial \vec{F}_1}{\partial \vec{V}_2}, \dots, \frac{\partial \vec{F}_1}{\partial \vec{V}_n} \\ \vdots \\ \frac{\partial \vec{F}_n}{\partial \vec{V}_1}, \frac{\partial \vec{F}_n}{\partial \vec{V}_2}, \dots, \frac{\partial \vec{F}_n}{\partial \vec{V}_n} \end{bmatrix} \tag{8}$$

The Jacobian matrix will be of dimensions: length($\vec{F}(\vec{V})$)×length($\vec{V}$). We can look at a single block matrix within this update term. Eq.(9) is the first arc and constraint assuming a full-state continuity.

$$\frac{\partial \vec{F}_1}{\partial \vec{V}_1} = \left[\frac{\partial(\vec{x}_{1,f} - \vec{x}_2)}{\partial \vec{x}_1}, \frac{\partial(\vec{x}_{1,f} - \vec{x}_2)}{\partial \Delta t_1} \right]_{6\times 7} \tag{9}$$

The already computed state transition matrix can be leveraged to define the partials of the integrated state ($\vec{x}_{1,f}$) with respect to the initial state ($\vec{x}_1$). Also, the partials of the integrated state with respect to time (Δt_1) is simply the velocity and acceleration of at the final state. With this in mind, we can rewrite Eq.(9) and the partial of the first constraint with respect to the second free variable state as:

$$\frac{\partial \vec{F}_1}{\partial \vec{V}_1} = \left[\Phi_1(\Delta t, 0), \dot{\vec{x}}_{1,f} \right]_{6\times 7} \qquad \frac{\partial \vec{F}_1}{\partial \vec{V}_2} = \left[-\mathbb{1}_{6\times 6}, \mathbb{0}_{6\times 1} \right]_{6\times 7} \tag{10}$$

This process is repeated for each free variable and constraint in the total $D\vec{F}(\vec{V})$ matrix. As stated earlier, we expect quadratic convergence in the solution. This is checked in the transfers presented in the next section.

A good discretization of each manifold for the multiple shooting scheme is imperative to ensuring a solution with low maneuver costs and relatively quick convergence. If arcs are too long, then the inherent linerization being used through the Jacobian will less accurately represent the true dynamics of the system. From testing with the transfers in this paper, an arbitrary 30 segments per manifold, 60 in total, was seen to be a good compromise between descent maneuver placement (not optimal by definition) and compute speed. This gives plenty of locations along the total trajectory to guess-and-check place maneuvers to reduce total ΔV costs and converge the solution in less than 10 iterations. Figure 9 shows an example of this discretization scheme applied to Trajectory 1A.

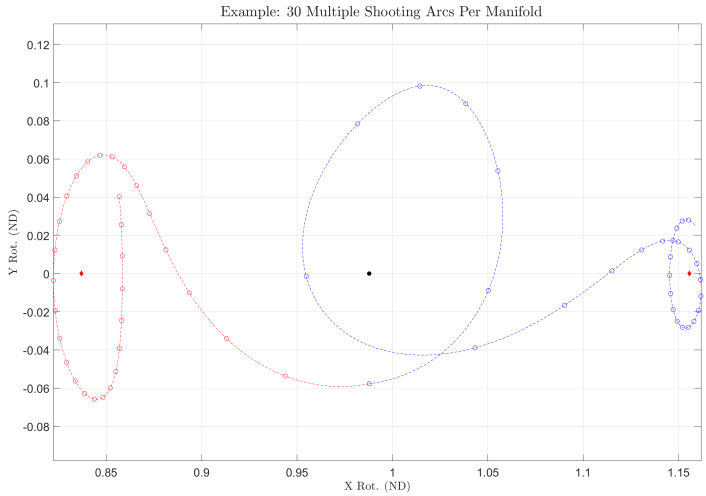

Figure 9: Example multiple shooting scheme with 30 segments per manifold.

4 Transfer Results

From the methods presented above and the mission design requirements, the following transfers were recovered. In this investigation, transfers will always originate and terminate at initial and final periodic orbit states. In a higher fidelity design, subsequent station keeping maneuvers would need to be performed to stay on a CR3BP defined periodic orbit. The following figures show each of the four cases recovered that meet the design criteria. All figures have color coded segments for further details. Red and blue dashed lines indicate the selected initial condition manifold. Red signifies an unstable manifold and thus is from the departing PO; Blue is the stable arrival manifold. Scatter points show where the multiple-shooting segments begin and terminate at the first iteration. The cyan continuous arc is the recovered solution after the multiple-shooting algorithm is within a tolerance value of $1e^{-10}$ for the norm of the constraint vector. For the plots, this cyan solution is independently propagated, always forwards in time, to ensure that the recovered solution from the multiple shooting algorithm is valid. The impulsive maneuvers are shown as red arrows along the trajectory in the direction of the burn. L1 and L2 are denoted by the red diamonds right and left of the Moon (black filled circle) respectively. Black direction of motion arrows are presented for clarity. Each transfer plot has an accompanying iteration count on the right subfigure. This plot demonstrates the multiple-shooting scheme's convergence to satisfying the norm of the constraint function. It serves as a good method to evaluate algorithm performance and ensure that the quadratic convergence we expect from Newton's method and the minimum-norm solution is seen. Once again, the terminal iteration's free-variable vector is independently propagated (cyan) to make sure the multiple shooting algorithm has truly recovered a valid solution.

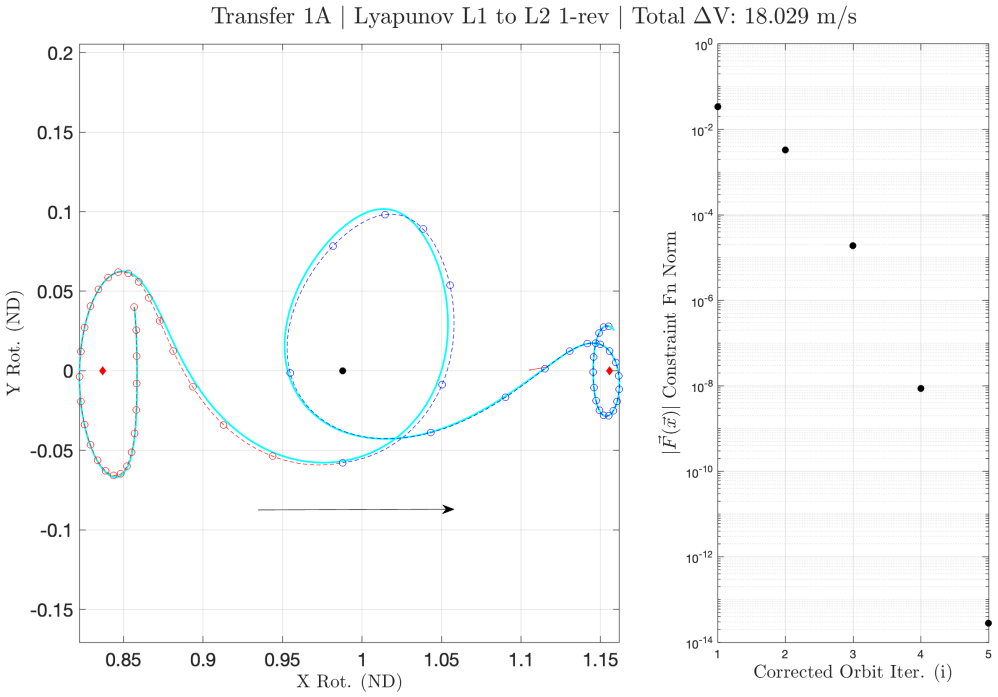

Figure 10: Transfer 1A is a L1 Lyapunov to L2 Lyapunov transfer.

Transfer 1A, seen in Figure 10, goes from a L1 Lyapunov with a Jacobi constant of 3.16916035196543 to a L2 Lyapunov that has a Jacobi constant of 3.17008882195783 and has a total of three maneuvers equaling 18.029 m/s. The first two occur in the close vicinity of the L1 Lyapunov which occur at 0.47 and 11.71 days into the flight. They have magnitudes of 2.15 and 4.42 m/s respectively. The revolution around the Moon is coasting and the final maneuver occurs before the loop into the L2 Lyapunov at 21.10 days with a magnitude of 11.45 m/s. The placement of these maneuvers can be moved around in future work to reduce the transfer cost, but their current guess-and-check placement has satisfied the 20 m/s total ΔV per transfer requirement. The time of flight for Transfer 1A is 37.72 days and the planar nature of this trajectory enables the mission requirements of the first mission category.

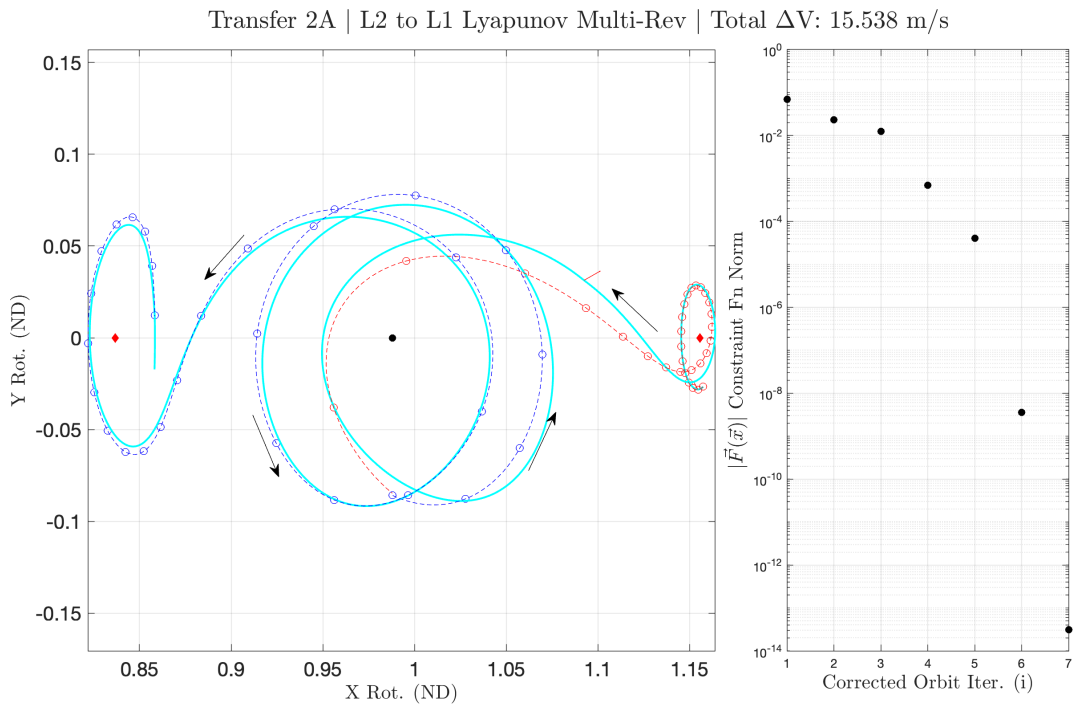

Figure 11: Transfer 2A is a L2 Lyapunov to L1 Lyapunov transfer.

Transfer 2A takes the spacecraft back to the L1 Lyapunov via a multi-revolution solution. The Jacobi constants for the departure and arrival periodic orbits are identical to Transfer 1A, but the manifolds used here are considerably different. The total flight time is 46.04 days and two maneuvers are located at 0.677 days and 18.56 days into the flight. These maneuvers have magnitudes of 5.06 and 10.47 m/s respectively. Placement of these maneuvers was varied with guess and check to try and reduce the total ΔV. This method was quite time consuming, but the results significantly reduced the cost compared to the first pass and satisfy the mission design requirements. With maneuvers placed at the beginning and end of each PO and at the intersection of the manifolds, the ΔV total was in excess of 80 m/s. The process of reducing this incorporated trial and error, moving one or more maneuvers along the trajectory to find better locations. This process isn't robust and still doesn't quite yield an optimal solution, but the total cost was reduced to 15.5 m/s. The terminal state along the transfer yields a Lyapunov periodic orbit that is stable for roughly 2 periods. This was of interest as initially a third maneuver was placed towards the end of the transfer to reach the terminal state exactly. However, the velocity discontinuity was so small that the maneuver would not even appropriately measured in mm/s. Therefore, the terminal state was propagated out for using the same integration tolerances as used to compute these transfers, to see how long the PO existed. It is important to note there will be a slight difference in this (and all the initial/terminal states) as these are along the manifolds for the POs and not the PO states themselves. In theory, a small maneuver would need to be performed, likely on the order of a fraction of a mm/s to join onto a truly periodic orbit in the CR3BP. To summarize, a third and final maneuver was not required in this case as the constraints were met and the terminal state propagated forwards in time remained in the vicinity of the L1 resembling a periodic orbit for a reasonable amount of time.

Transfer 1B, shown in Figure 12, starts at an L1 Northern Halo orbit, Jacobi constant of 3.17360488574852, and terminates on a L2 Southern Halo orbit, Jacobi constant of 3.15183826360119, with a total flight time of 37.8 days. Both have their inclination with respect to the X/Y-plane formed from the Earth-Moon orbit and can be seen in Figure 13. This inclination satisfies the loose requirement for "higher latitudes" accessibility for science observation on either side of the moon. Transfer 1B has a total of four maneuvers totalling 59.8 m/s of ΔV. These maneuvers are placed 3.2, 14.1, 23.7, and 33.1 days into the transfer. Maneuvers 1 and 2 are 10 and 38 m/s and 3 and 4 are 6.7 and 5 m/s. This transfer requires more ΔV than the first case due to matching additionally out-of-plane components of states and likely sub optimal maneuver placement. Maneuvers 1, 3, and 4 are primarily out-of-plane. Lunar

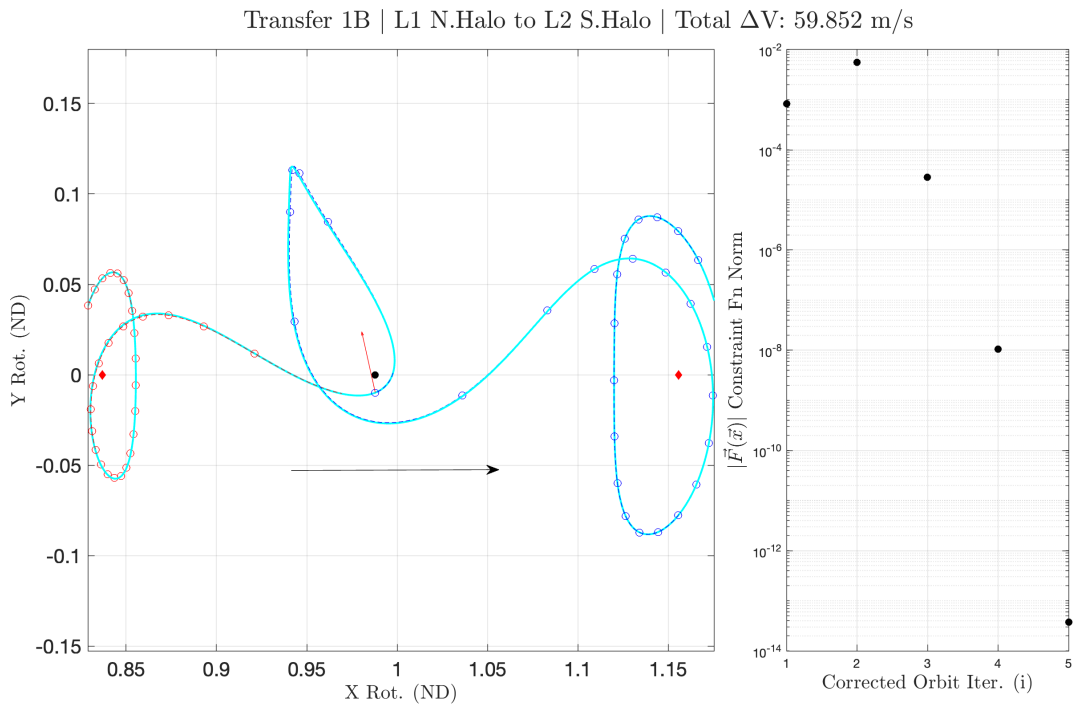

Figure 12: Transfer 1B is a L1 Northern Halo to L2 Southern Halo transfer.

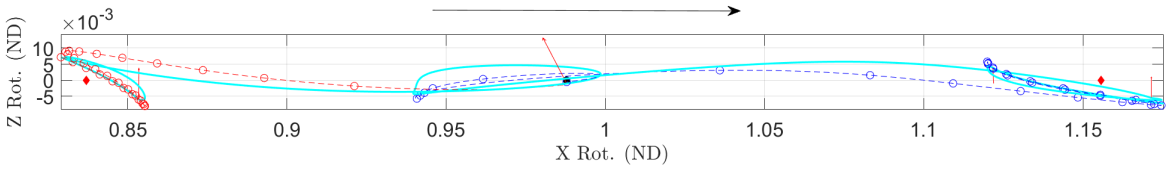

Figure 13: Transfer 1B seen from the ND X/Z-Plane

conjunctions occur twice along this transfer and are shown in Figure 16. The first begins 14.17 days into the transfer and lasts for 0.644 hours. The second occurs at 31.51 days lasting for 3.055 hours. These values were calculated by finding comparing the tangent angle between y/z coordinate norm and the x-distance from Earth (not the system barycenter) to the radius of the moon and the x-distance from Earth. If the angle is less than the latter, then the spacecraft is considered to be out-of-view from the Earth. In theory, this value will change slightly due to ground station latitudes on Earth, but for this study this isn't considered. This transfer satisfies the second mission requirements.

Transfer 2B returns the spacecraft back to the Northern L1 Halo from the Southern L2 Halo and thus has the same Jacobi constants for the initial and final periodic orbits as the ones presented in Transfer 1B. As discussed in the Transfer Selection section of the paper, this trajectory requires several revolutions around the Moon prior to arrival. This is evident in the figure as well as the fact that the time of flight is 45.68 days long. Early into the transfer (0.68 days) the first maneuver of 0.75 m/s is performed to have the spacecraft ever-so-slightly depart the manifold trajectory. This is followed by a larger 7.06 m/s maneuver 10.85 days into the flight which occurs roughly at the bottom of the first "bean shape" around the L2. There is a sharp kink in the trajectory occurring at around 17 days into the flight. This is likely due to the relative velocity of the spacecraft approaching that of the rotating frame to appear "motionless" for a brief period along the trajectory. At 19.9 days the largest maneuver occurs which is 42.48 m/s. This considerably changes the spacecraft's energy compared to the other maneuvers. Finally, one more maneuver occurs mostly out-of-plane at 41.56 days with a magnitude of 8.5 m/s. While the increased revolutions around the moon potentially increases the number of conjunction conditions, in testing for this trajectory, only two instances are seen. These are in Figure 16 on the bottom subfigure. These conjunction conditions occur at 13.42 days and 30.97

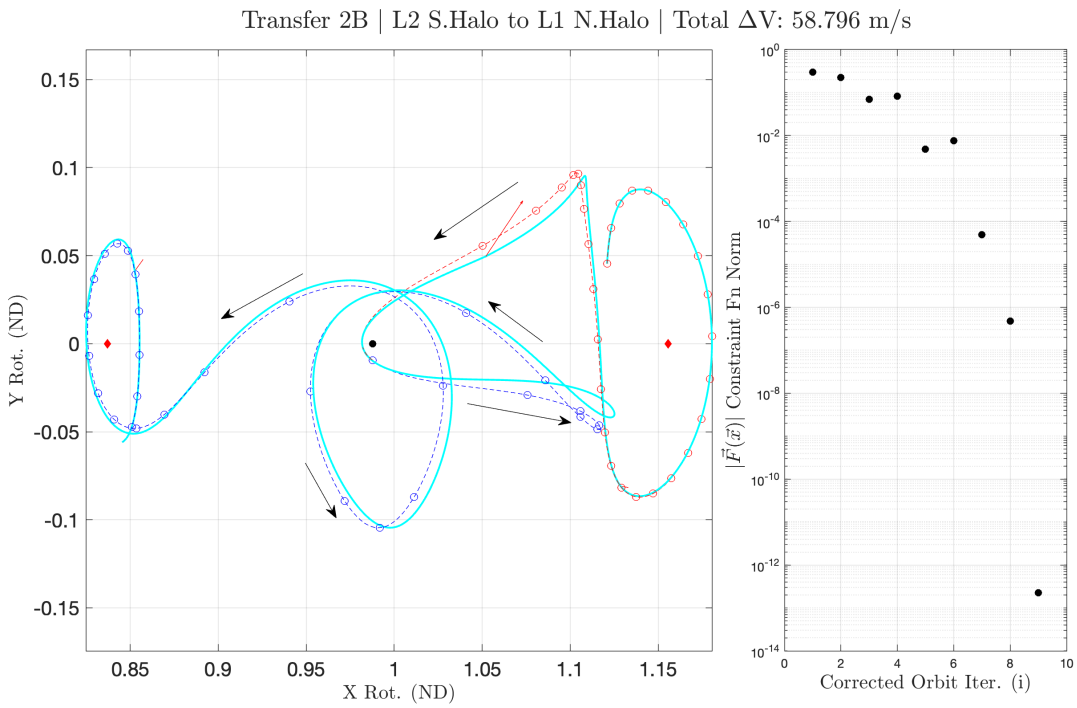

Figure 14: Transfer 2B the return trajectory from 1B and goes between the L2 Southern Halo to L1 Northern Halo periodic orbits.

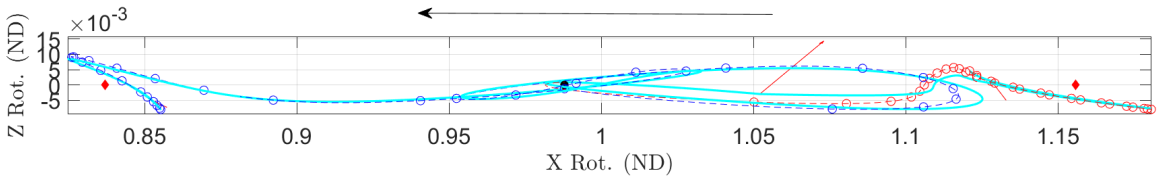

Figure 15: Transfer 2B seen from the ND X/Z-Plane

days with durations of 4.33 and 1.13 hours respectively. Both are under the 5 hour maximum and thus satisfy the mission requirement.

Each of the solutions presented above have their Jacobi constant versus non-dimensional time plotted in Figure 17. The changes in Jacobi constant are instantaneous due to the impulsive maneuvers. In each of the trajectories it is apparent that a small maneuvers are done close to the initial and terminal periodic orbits. Particularly in Transfer 1B and 2B, the largest maneuver occurs roughly in the middle of the transfer and has a magnitude considerably larger than the rest of the maneuvers. This can likely be modified in future work to place larger maneuvers earlier and later in the trajectory to try and bring down the large cost in the middle of the transfer.

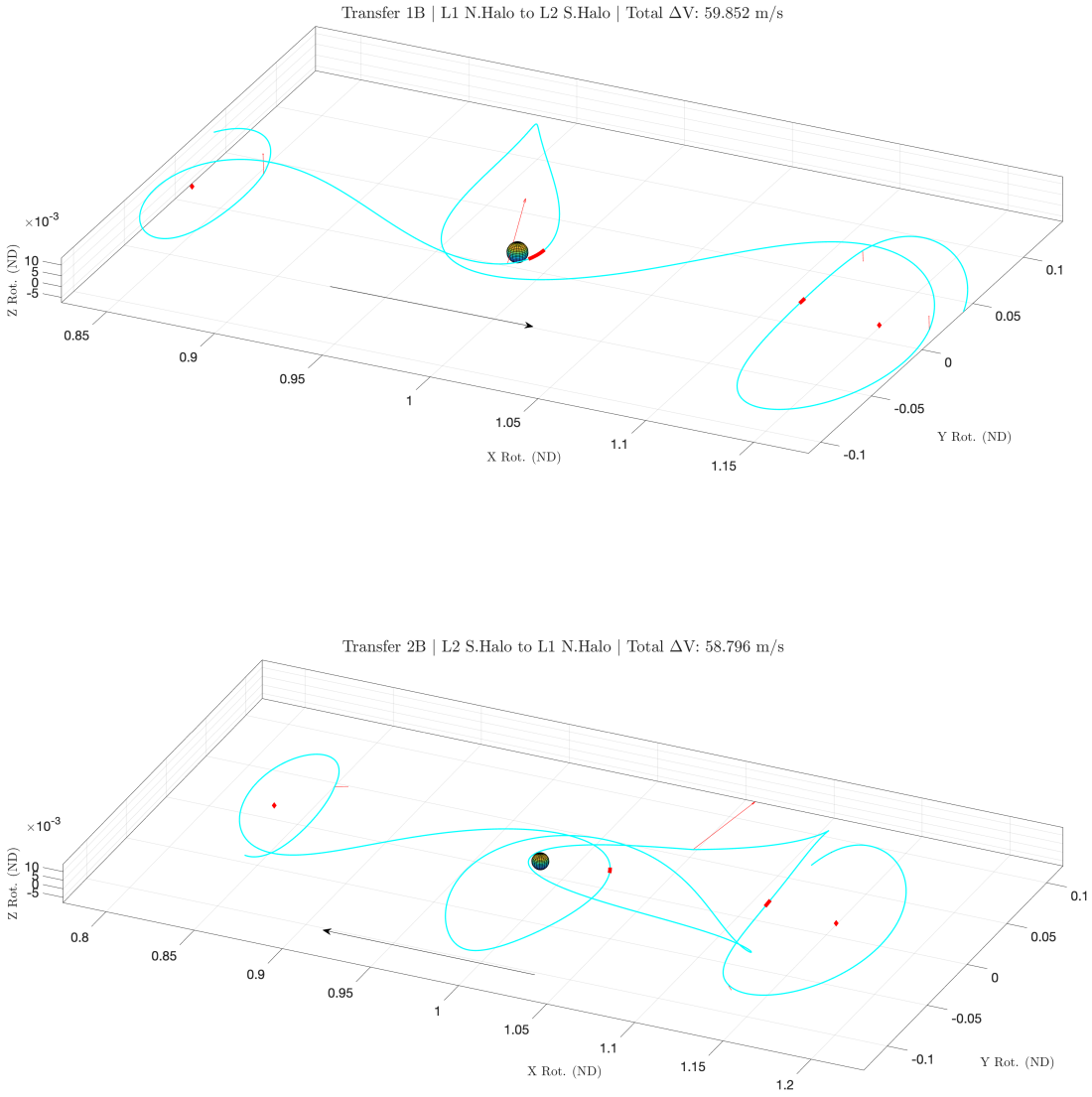

Figure 16: Transfer 1B and 2B with Lunar conjunction conditions highlighted in red along the trajectory. The ND radius of the Moon is also shown which makes it evident that both transfers have very close perilunes.

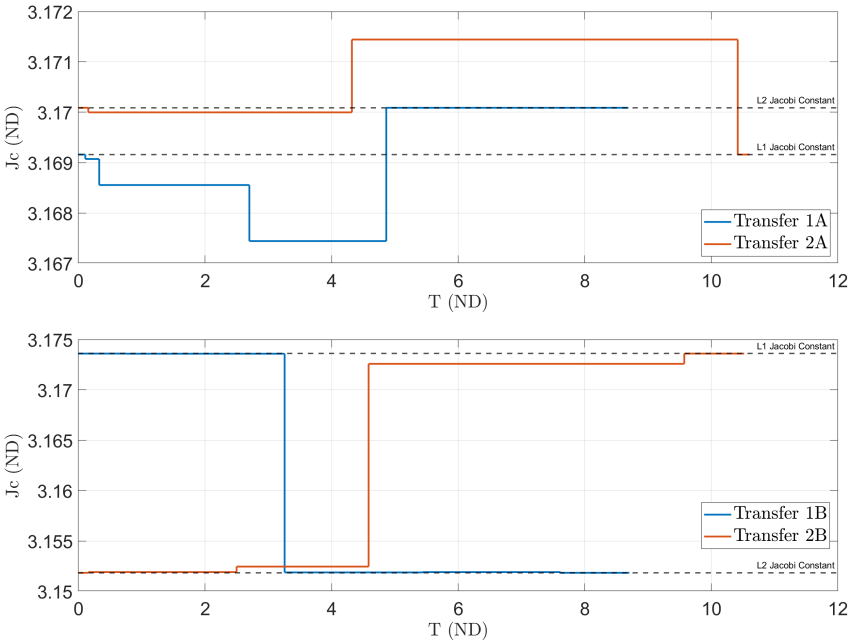

Figure 17: Transfers Jacobi constant versus non-dimensional time.

5 Conclusion and Future Work

The trajectories shown in this paper demonstrate transfers from one periodic orbit to another in the Earth-Moon system. Specifically, the Lyapunov and Halo periodic orbit families are investigated about the system's L1 and L2 Lagrange points. In order to model these trajectories and satisfy the problem motivation, the dynamical model is discussed and specific properties of periodic orbits, namely their departure and arrival manifolds, are used to find good initial guesses. Inherently each trajectory must pass through the x-coordinate of the Moon in the CR3BP, hence this makes for a good location to sample various manifolds emanating from either periodic orbit to visually minimize position and velocity discontinuities. The resulting initial guess trajectories are then corrected using a multiple shooting scheme that allows for velocity discontinuities at specified locations to incorporate impulsive maneuvers.

The process yields trajectories that satisfy the objectives of this survey. First, Earth-Moon planar transfers are accomplished from Trajectories 1A and 2A which take the spacecraft between L1 and L2 Lyapunov periodic orbits of dissimilar Jacobi constants. Trajectory 1B and 2B demonstrate the capability of Halo to Halo transfers where both trajectories have Lunar conjunction durations less than 5 hours in length. These transfers return to the same periodic orbits, thus can be consistently used to have the spacecraft shift between these Lagrange points for their science orbits.

The trajectories presented above are by no means optimal. Future work regarding this problem includes a more comprehensive search space evaluation prior to creating transfers. By specifically studying different kinds of energy levels of periodic orbits, their manifolds, and multi-revolution solutions, a more optimal set of initial and final periodic orbits is likely to be achieved. Heteroclinic connections also exist in this system, and so these can be investigated and incorporated save on maneuver costs. Finally, better maneuver placement is critical to reducing costs. From the limited trial-and-error testing presented above, it was demonstrated that significant cost savings are possible with a bit of maneuver placement planning. This can be achieved through adding segments in specific locations along the trajectory. Using a direct optimization scheme with a total ΔV cost function here is likely the best way to approach this problem. If the propulsion model can be modified, possibly incorporating low-thrust optimal transfers can also yield cost savings. Finally, candidate transfers can be modeled in higher fidelity dynamical environments through software tools such as NASA's General Mission Analysis Tool (GMAT) or AGI's Satellite Toolkit (STK). The CR3BP solutions presented here and from future work would be good starting points for this model.